


Antihydrogen formation from laser-assisted antiproton-positronium collisions

K. Lévêque-Simon* and P.-A. Hervieux†

Université de Strasbourg, CNRS, Institut de Physique et Chimie des Matériaux de Strasbourg, UMR 7504, F-67000 Strasbourg, France

 (Received 7 December 2022; accepted 8 May 2023; published 30 May 2023)

The formation of antihydrogen atoms from three-body collisions between positronium atoms and antiprotons plays a crucial role in the gravitational behavior of antihydrogen at rest (GBAR) experiment devoted to the measure of the action of gravity on antimatter. One of the main challenges facing this experiment is to find the means for increasing the production of antihydrogens which are produced by the reaction $\bar{p} + \text{Ps} \rightarrow \bar{\text{H}} + e^-$ with an extremely low rate. Along these lines, we investigate here the possibility to influence the collision process by using a laser field. A perturbative approach combining the Coulomb-Born approximation for modeling the charged-particle collision and a first-order perturbation theory for describing laser-atom interactions is employed to estimate laser-mediated charge-exchange cross sections. By carefully considering the laser specifications compatible with the experimental constraints, we present an extensive study of the influence of the laser parameters (laser wavelength and intensity) on the cross sections in the energy range of interest for GBAR. We show that under special irradiation conditions the rate of antihydrogen production may be significantly increased by the presence of the laser field.

DOI: [10.1103/PhysRevA.107.052813](https://doi.org/10.1103/PhysRevA.107.052813)

I. INTRODUCTION

In order to make a direct observation of the effect of gravitation on antimatter, the gravitational behavior of antihydrogen at rest (GBAR) experiment aims at measuring the influence of earth's gravity on the trajectory of cold antihydrogen atoms. We mention two other experiments, AEGIS [1,2] and ALPHA-g [3], which are designed to realize the same objective as the GBAR experiment. In the first stage of the GBAR experiment, positively charged ions of antihydrogen $\bar{\text{H}}^+$ (one antiproton and two positrons) are produced with the help of two successive low-energy collisions [4,5]. The first reaction is a charge-exchange three-body collision (a) $\bar{p} + \text{Ps}(n_p, l_p) \rightarrow \bar{\text{H}}(n_h, l_h) + e^-$, where \bar{p} stands for antiproton, $\text{Ps}(n_p, l_p)$ for positronium [bound states of an electron and a positron characterized by the quantum numbers (n_p, l_p)], and $\bar{\text{H}}(n_h, l_h)$ for antihydrogen in the state (n_h, l_h) . The second one is a more complex four-body reaction (b) $\text{Ps}(n_p, l_p) + \bar{\text{H}}(n_h, l_h) \rightarrow \bar{\text{H}}^+ + e^-$. In view of the extremely low production rate of $\bar{\text{H}}^+$, the current challenge is to optimize each element of the experiment. In this spirit, we analyze theoretically the possibility to increase the production rates of the antihydrogen atoms, by assisting reaction (a) with a laser. In addition, reaction (a) has already been widely explored with a large variety of theoretical models in the non-light-assisted situation (see [6–11] and references therein). These theoretical studies show that antihydrogen atoms would be mainly produced in excited states and the use of excited states of positronium instead of the ground state allows one to increase the production of antihydrogen. In the light-assisted situation,

the recombination process of an electron with a proton by using a semiclassical approach has been explored [12].

The main motivation of this work is related to the fact that since the atomic excited states are less bound compared to their ground-state counterparts one may expect to have a reaction more sensitive to the presence of an external laser field. In the following, cross sections for reaction (a) are obtained in the antiproton energy range of the GBAR experiment (1–10 keV), by using a semiperturbative approach adapted from [6,13–15]. This method allows the simultaneous treatment of the electron-atom interaction (within the Coulomb Born approximation), the electron-laser interaction (Volkov states), and the laser-atom interactions (within the first-order time-dependent perturbation theory). In order to model the interaction with light, we only consider quasisonant excitation conditions of the positronium leading to optimal situations for laser-assisted antiproton-positronium collisions. By considering commercially available lasers whose wavelengths are around 243 nm (Lyman- α transition) and 2563 nm (Paschen- β transition), Ps excitation by the one-photon transition from 1s, 3s, and 3d states has been considered. Moreover, an important issue related to the GBAR experiment is the fact that the positronium atoms are produced with a velocity distribution leading to first-order Doppler shifts. The latter must be taken into account in the description of the collision process. Finally, laser wavelengths and intensities must be chosen in order to be compatible with the theoretical framework and also to avoid the breakdown (by ionization) of the atomic species implied in the collision.

Concerning the organization of this paper, the details of our theoretical model are described in the next section. The results and discussion are given in Sec. III. We summarize in Sec. IV and discuss some perspectives for future work. Atomic units are used unless specified otherwise.

*kevin.leveque-simon@sorbonne-universite.fr

†hervieux@unistra.fr

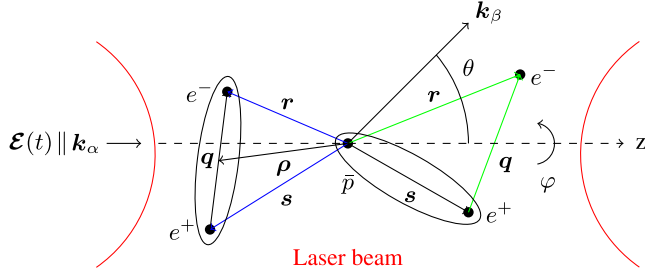


FIG. 1. Coordinates used for reaction (a). The bound states present in each channel (entrance and exit) are circled: The dark blue and light green straight lines correspond to the short-range perturbative potential in prior and post forms, respectively. The scattering angle is defined by $\theta = (\hat{k}_\alpha, \hat{k}_\beta)$ and the laser beam plane is shown in red.

II. THEORETICAL METHODS

Let us consider the laser-assisted three-body reaction (a) $\bar{p} + \text{Ps}(n_p, l_p) - p\omega_0 \rightarrow \bar{H}(n_h, l_h) + e^-$, where positive integer values of p correspond to photon emission by the three-body particle system, negative ones to photon absorption, and $p = 0$ to a laser-assisted collision process with no net transfer of photons between the system of particles and the field. In the following we assume that the laser is treated classically as a spatially homogeneous electric field (i.e., dipole approximation), linearly polarized with a single mode $\mathcal{E}(t) = \mathcal{E}_0 \sin(\omega_0 t) \hat{z}$. This description is justified within the limits described as follows.

(i) The pulse durations that we consider (higher than 1 ps) are sufficiently long so that, on average, the laser intensity does not vary much from its peak intensity on timescales that are of the order of typical subfemtosecond collision times. As a result, the scattering process is described in terms of time-independent transition rates [14,16].

(ii) The radiation generated by a laser in a coherent state is close to the classical state of the field for a large number of photons [17]. This is because for large values of the average number of photons in the coherent state, quantum corrections only cause small fluctuations on the classical field. Given the laser parameters used in this paper, this approximation is more suitable to simulate the excitation of positronium prepared in an excited state than this one is in the ground state.

As depicted in Fig. 1, the incident positronium momentum is defined by \mathbf{k}_α and is z axis oriented, the ejected-electron momentum is defined by \mathbf{k}_β , and the electric field of the laser pulse \mathcal{E} is taken to be parallel to the incident positronium momentum. We begin by considering the case for which the ejected electron is fast so that the electron-atom interaction can be treated perturbatively by using the first Born approximation [14]. In addition, the Coulomb distortions [see [18] for the details of this approximation, called the continuum distorted-wave initial-state (CDW-IS) approximation] in the entrance channel due to the incoming electron and positron in the continuum of the residual proton are not included here. The Coulomb Born approximation (CBA), meaning that plane waves are used to describe the propagation of the incoming electron and positron, is preferred. This is due to the fact that the comparison between experimental data [19] and previous

results obtained using a zero-field approach by Comini *et al.* [20] suggests that the CBA is more convenient than the CDW-IS approximation in the case of ground-state positronium, which is our main concern here.

Since in rearrangement collisions the particles are different in the initial and final states, the interaction potential in the exit channel is different from the one in the entrance channel. Therefore, when writing the \mathcal{S} -matrix elements, a choice has to be made between the perturbing potential of the initial state and the one of the final state. The prior form of the \mathcal{S} -matrix elements is given by [21]

$$\mathcal{S}_{k_\beta, k_\alpha}^{\text{CBA}} = -i \int_{\mathbb{R}} dt \langle \Phi_{k_\beta}(t) | V_\alpha | \Phi_{k_\alpha}(t) \rangle, \quad (1)$$

where $V_\alpha(\mathbf{r}, \mathbf{s}) = |\mathbf{r}|^{-1} - |\mathbf{s}|^{-1}$, with \mathbf{r} and \mathbf{s} the coordinates of the electron and the positron, respectively (see Fig. 1). It is worth mentioning that the same transition matrix elements are obtained using the *prior* and *post* forms of Eq. (1) if the asymptotic states embedded in the laser field $|\Phi_{k_\alpha}(t)\rangle$ and $|\Phi_{k_\beta}(t)\rangle$ are the exact eigenstates of the initial and final Hamiltonians, respectively. Therefore, no post-prior discrepancies occur on the zero-field cross sections in the Coulomb Born approximation. Regarding the discrepancies on the CBA cross sections in the presence of a laser field, they cannot be prevented, as the method used to deal with the laser-atom interactions leads to approximate eigenstates of the initial and final Hamiltonians. By neglecting the effect of the external field on the heavy antiparticle \bar{p} since $m_{\bar{p}} \sim 1836m_e$, one needs to determine the dressed states of the atoms and of the ejected electron for the computation of Eq. (1). Because the treatment for the atoms is the same in the two channels, the positronium has been selected arbitrarily to illustrate the analytical approach employed.

The asymptotic initial state is described by the time-dependent Schrödinger equation

$$i\partial_t |\Phi_{k_\alpha}(t)\rangle = [\mathcal{H}_\alpha(\mathbf{r}, \mathbf{s}) + \mathcal{H}_I(\mathbf{r}, \mathbf{s}, t)] |\Phi_{k_\alpha}(t)\rangle, \quad (2)$$

$$\mathcal{H}_\alpha(\mathbf{r}, \mathbf{s}) = -\frac{1}{2}(\Delta_r + \Delta_s) - |\mathbf{r} - \mathbf{s}|^{-1}, \quad (3)$$

$$\mathcal{H}_I(\mathbf{r}, \mathbf{s}, t) = i\alpha(\nabla_s - \nabla_r) \cdot \mathbf{A}(t) + [\alpha A(t)]^2, \quad (4)$$

where \mathcal{H}_α is the initial unperturbed Hamiltonian, \mathcal{H}_I is the interaction term of the entrance channel, and $\alpha \sim \frac{1}{137}$ a.u. is the fine-structure constant. In Eq. (3) the separation of the Ps center of mass can be performed by introducing the coordinates $\boldsymbol{\rho} = \frac{1}{2}(\mathbf{r} + \mathbf{s})$ and $\mathbf{q} = \mathbf{r} - \mathbf{s}$ shown in Fig. 1. The use of this new set of coordinates allow us to write

$$\mathcal{H}_\alpha(\boldsymbol{\rho}, \mathbf{q}) \equiv \mathcal{H}_\alpha^\rho(\boldsymbol{\rho}) + \mathcal{H}_\alpha^q(\mathbf{q}) = -\frac{1}{4}\Delta_\rho - \Delta_q - \frac{1}{q}, \quad (5)$$

where the corresponding eigenfunctions are given by [22]

$$\Phi_{k_\alpha}(\mathbf{q}, \boldsymbol{\rho}, t) = (2\pi)^{-3/2} e^{i(\mathbf{k}_\alpha \cdot \boldsymbol{\rho} - v^2 t)} e^{-i\alpha A(t) \cdot (\mathbf{r} - \mathbf{s})} \xi_\alpha^L(\mathbf{q}, t). \quad (6)$$

In this equation the first factor describes the motion of the center of mass characterized by the incident momentum $\mathbf{k}_\alpha = 2v\hat{z}$, where v is the impact velocity. So far we have assumed that the antiproton is at rest. However, by using the formula $v^2 \sim 2E_{\bar{p}}/m_{\bar{p}}$ we can investigate the situation where the positronium is at rest and the antiproton is in motion. The second factor of Eq. (6) is related to the Göppert-Mayer

gauge transformation, which ensures that the Hamiltonian $\mathcal{H}_I^L(\mathbf{q}, t) = \mathcal{E}(t) \cdot \mathbf{q}$ is obtained in the length gauge by removing the A^2 term in Eq. (4). Finally, the last factor of Eq. (6) corresponds to the positronium dressed state that satisfies the time-dependent Schrödinger equation [we use $\mathcal{E}(t) = -\alpha \partial_t A(t)$]

$$i\partial_t |\xi_\alpha^L(t)\rangle = [\mathcal{H}_\alpha^q(\mathbf{q}) + \mathcal{H}_I^L(\mathbf{q}, t)] |\xi_\alpha^L(t)\rangle. \quad (7)$$

In what follows we consider electric-field strengths such as $\mathcal{E}_0 \ll e/a_0^2 = 5.142 \times 10^9$ V/cm (the atomic unit of field strength). The positronium dressed states can then be obtained by use of first-order time-dependent perturbation theory [13]. In particular, the solutions of Eq. (7) are expressed as

$$|\xi_\alpha^L(t)\rangle = e^{-i\epsilon_{n_p} t} [|\psi_{n_p}\rangle + i(|v_{n_p}^+\rangle e^{i\omega_0 t} - |v_{n_p}^-\rangle e^{-i\omega_0 t})] + O(\mathcal{E}_0^2), \quad (8)$$

$$|v_{n_p}^\pm\rangle = \frac{1}{2} \left(\sum_n \frac{|\psi_n\rangle \langle \psi_n|}{\epsilon_n - \epsilon_{n_p} \pm \omega_0} + \int_{\mathbb{R}^3} d\boldsymbol{\kappa} \frac{|\psi_\kappa\rangle \langle \psi_\kappa|}{E_\kappa - \epsilon_{n_p} \pm \omega_0} \right) \times \mathcal{E}_0 \cdot \mathbf{q} |\psi_{n_p}\rangle, \quad (9)$$

where $\langle \psi_n | \mathcal{E}_0 \cdot \mathbf{q} | \psi_{n_p} \rangle$ are the dipole-coupling matrix elements. The states $|\psi_n\rangle$ are those of a hydrogenoid atom of reduced mass $\mu = \frac{1}{2}$ in the absence of the laser field with binding energies of $\epsilon_n = -\mu/2n^2$. Moreover, the time-independent states $|v_{n_p}^\pm\rangle$ obtained at first order in the perturbation are expanded in terms of the eigenbasis (including bound and continuum states) of the reduced Hamiltonian \mathcal{H}_α^q (i.e., the Coulomb eigenstates $|\psi_\kappa\rangle$ describing the motion of the electron with wave vector $\boldsymbol{\kappa}$ and positive energy $E_\kappa = \kappa^2/2\mu$ moving in the continuum of the residual positron). With the help of the spectral representation of the Coulomb Green's function [23], the position representation of time-independent states (9) can be written as

$$v_{n_p}^\pm(\mathbf{q}) = -\frac{1}{2} \int_{\mathbb{R}^3} d\mathbf{q}' G_c(\epsilon_{n_p} \mp \omega_0, \mathbf{q}, \mathbf{q}') \mathcal{E}_0 \cdot \mathbf{q}' \psi_{n_p}(\mathbf{q}'). \quad (10)$$

The details of the method employed to compute Eq. (10) are given in Appendix A. Similarly, the wave function corresponding to the asymptotic final state can be written as

$$\Phi_{k_\beta}(\mathbf{r}, \mathbf{s}, t) = e^{i\alpha A(t) \cdot \mathbf{s}} \xi_\beta^L(\mathbf{s}, t) \chi_{k_\beta}(\mathbf{r}, t), \quad (11)$$

where the antihydrogen states dressed by the laser field $|\xi_\beta^L(t)\rangle$ can be expressed as

$$|\xi_\beta^L(t)\rangle = e^{-i\epsilon_{n_h} t} [|\psi_{n_h}\rangle - i(|v_{n_h}^+\rangle e^{i\omega_0 t} - |v_{n_h}^-\rangle e^{-i\omega_0 t})] + O(\mathcal{E}_0^2). \quad (12)$$

With respect to the Ps case of Eq. (8), one notes (i) a change of sign in front of the imaginary unit which comes from a gauge fixing in Eq. (11) and (ii) that the unperturbed wave functions $|\psi_{n_h}\rangle$ are obtained by using $\mu = 1$ in the general expression of the hydrogenic wave functions.

In contrast, the laser-electron interaction χ_{k_β} can be treated exactly by using the nonrelativistic version of the Gordon-Volkov wave function [24,25], which is a solution of the time-dependent Schrödinger equation with the Hamiltonian

$\frac{1}{2}[-i\nabla_r + \alpha A(t)]^2$. The complete expression is

$$\chi_{k_\beta}(\mathbf{r}, t) = (2\pi)^{-3/2} e^{-(i/2)k_\beta^2 t + ik_\beta \cdot [\mathbf{r} - \mathbf{d}(t)] - i\phi(t)}, \quad (13)$$

$$\mathbf{d}(t) = \alpha \int_{-\infty}^t A(t') dt' = \frac{\mathcal{E}_0}{\omega_0^2} \sin(\omega_0 t) \hat{\mathbf{z}}, \quad (14)$$

$$\phi(t) = \frac{1}{2} \alpha^2 \int_{-\infty}^t A^2(t') dt' = \langle U \rangle t + \frac{1}{8} \frac{\mathcal{E}_0^2}{\omega_0^3} \sin(2\omega_0 t), \quad (15)$$

where $A(t) = \mathcal{E}_0 \cos(\omega_0 t)/\alpha\omega_0$ is the vector potential expressed in the Coulomb gauge (automatically satisfied in the dipole approximation). The quantum evolution of the electron in the laser field (13) is a superposition of a quiver motion and a drift motion [14]. The quiver motion corresponds to the displacement $|\mathbf{d}(t)|$ (14) of the electron from its oscillation center along the polarization direction $\hat{\mathbf{z}}$. The drift motion, which involves the cycle-averaged quiver energy of a free electron in the laser field $\langle U \rangle = \frac{1}{4}(\mathcal{E}_0/\omega_0)^2$ (i.e., ponderomotive energy) and cannot be described in the dipole approximation, corresponds to a displacement $\alpha\phi_0(t)$ (15) along the propagation direction of the field.

At this point it is important to note the following. On the one hand, the dressed atomic states have been obtained at the lowest order of the time-dependent perturbation theory (8) and (12) and, according to the theory of multiphoton processes, are thus valid only for an exchange of one photon between the atoms and the field. On the other hand, the dressed-electron state can be described exactly by the Gordon-Volkov wave function, which is therefore able to represent the electron quantum motion in the exit channel, regardless of the number of photons absorbed or emitted between the field and the outgoing electron.

Inserting Eqs. (6) and (11) into Eq. (1), we obtain

$$\mathcal{S}_{k_\beta, k_\alpha}^{\text{CBA}} = -(2\pi)^{-3} i \int_{\mathbb{R}^6} d\mathbf{r} d\mathbf{s} e^{i(\mathbf{k}_\alpha \cdot \boldsymbol{\rho} - \mathbf{k}_\beta \cdot \mathbf{r})} V_\alpha(\mathbf{r}, \mathbf{s}) \times \int_{\mathbb{R}} dt e^{i\gamma(\mathbf{r}, t)} \xi_\beta^{L*}(\mathbf{s}, t) \xi_\alpha^L(\mathbf{q}, t), \quad (16)$$

where the time-dependent phase is defined by

$$\gamma(\mathbf{r}, t) \equiv \gamma_0 t + \gamma_1(\mathbf{r}, t), \quad (17)$$

$$\gamma_0 = \frac{1}{2} k_\beta^2 + \epsilon_{n_h} - v^2 - \epsilon_{n_p}, \quad (18)$$

$$\gamma_1(\mathbf{r}, t) = \alpha_l \sin(\omega_0 t) - \beta_l \sin\left(\omega_0 t + \frac{\pi}{2}\right) + \gamma_l \sin(2\omega_0 t) + \langle U \rangle t. \quad (19)$$

In these relations, γ_0 is the phase factor derived from the energy conservation law for the zero-field case and γ_1 is the additional term generated by the external field. The dimensionless electron-field coupling parameters which appear in Eq. (19) are defined by $\alpha_l = \mathcal{E}_0 \cdot \mathbf{k}_\beta / \omega_0^2$, $\beta_l = \mathcal{E}_0 \cdot \mathbf{r} / \omega_0$, and $\gamma_l = \mathcal{E}_0^2 / 8\omega_0^3$, respectively. Using the Jacobi-Anger expansion, the field-dependent exponential term of Eq. (16) can be rewritten in terms of an infinite series involving one- and two-dimensional Bessel functions [26]

$$e^{i\gamma_1(\mathbf{r}, t)} = e^{i\langle U \rangle t} \sum_{k, q=-\infty}^{\infty} J_k(\alpha_l, \gamma_l) J_q(\beta_l) e^{i[k\omega_0 t - q(\omega_0 t + \pi/2)]}. \quad (20)$$

In order to reduce the double sum to a single one the change of variable $p = q - k$ is performed in Eq. (20) along with the use of Graf's addition theorem, which leads to [27,28]

$$e^{i\gamma_l(\mathbf{r}, t)} = e^{i(U)t} \sum_{p=-\infty}^{\infty} e^{ip\omega_0 t} \chi_p \sum_{k=-\infty}^{\infty} (-1)^k \times J_{p-2k}(c_l) J_k(\gamma_l) e^{-i(p-2k)\xi_l}, \quad (21)$$

where p , as already mentioned, corresponds to the number of photons exchanged between the system of particles and the field. The coefficients that appear in Eq. (21) are defined by

$$\chi_p = e^{-ip(\pi/2)[1-\text{sgn}(\alpha_l/\beta_l)]}, \quad (22)$$

$$c_l = \sqrt{\alpha_l^2 + \beta_l^2}, \quad (23)$$

$$\xi_l = \arctan(\beta_l/\alpha_l). \quad (24)$$

At this stage, the continuation of analytical calculations is not feasible since the argument of the Bessel functions involved in Eq. (21) is coordinate dependent. For this reason, we consider the approximation employed in the low-frequency regime, which consists, through Eq. (23), in neglecting the contribution of β_l relative to the one of α_l . To roughly estimate the error induced by this approximation on the argument of coordinate-dependent Bessel functions, we start by estimating the ratio $|\beta_l/\alpha_l|$ by $\omega_0(r)(k_\beta)^{-1}$. The latter is defined in terms of the average Ps Bohr radii $\langle r \rangle$ [29]. In the case of $\bar{H}(1s)$ and using the laser parameters considered in Sec. III, this ratio is equal to (i) 0.33 for Ps(1s) with $\omega_0 \sim 0.1875$ a.u. at an antiproton energy of 10 keV and (ii) 0.37 for Ps(3d) with $\omega_0 \sim 0.0178$ a.u. at an antiproton energy of 1 keV, respectively. It ensues that the argument can be estimated as $c_l \sim |\alpha_l|(1 + \frac{1}{2}|\beta_l/\alpha_l|^2)$, leading to $1.054|\alpha_l|$ for (i) and $1.068|\alpha_l|$ for (ii). Therefore, considering the low-frequency approximation, which implies that $c_l \sim |\alpha_l|$ and $\xi_l \sim \beta_l/\alpha_l \equiv \boldsymbol{\kappa} \cdot \mathbf{r}$ with $\boldsymbol{\kappa} = \boldsymbol{\mathcal{E}}_0/\alpha_l\omega_0$, induces an error of the order of 10% on the argument of the coordinate-dependent Bessel functions. This error is comparable to the uncertainties of the intensities delivered by the laser sources in the experiments. Moreover, the phase factor χ_p in Eq. (21) which does not affect the cross-section calculations can be omitted. The infinite sum over k can also be simplified due to the behavior of Bessel functions $J_k(\gamma_l) \sim \delta_{0k}$ for small values of γ_l , which currently does not exceed 10^{-6} a.u. The integrations over time and space are now fully separable. The integration over time leads to a δ function, and retaining only the lowest order in the field strength in the product of the atomic dressed states, the \mathcal{S} -matrix elements can be recast in the form

$$S_{k_\beta, k_\alpha}^{\text{CBA}} = -2i\pi \sum_{p=-\infty}^{\infty} \delta(\gamma_0 + \langle U \rangle + p\omega_0) \mathcal{T}_p^{\text{CBA}}. \quad (25)$$

In these relation, $\mathcal{T}_p^{\text{CBA}} \equiv \mathcal{T}_p^1 + \mathcal{T}_p^2 + \mathcal{T}_p^3$ is the Floquet \mathcal{T} -matrix elements which describe the transfer of p photons between the system of particles and the field in the Coulomb Born approximation. The partial components \mathcal{T}_p^j , which represent the effect of the field on the electron ($j = 1$), the

positronium ($j = 2$) and the antihydrogen ($j = 3$), respectively, are given by

$$\mathcal{T}_p^j(\mathbf{k}_\beta) = (2\pi)^{-3} \int_{\mathbb{R}^6} d\mathbf{r} ds e^{i[(v-k_\beta)\cdot\mathbf{r} + v\cdot\mathbf{s}]} V_\alpha(\mathbf{r}, \mathbf{s}) h_p^j(\mathbf{r}, \mathbf{s}), \quad (26)$$

$$h_p^1 = J_p(|\alpha_l|) e^{-ip\boldsymbol{\kappa}\cdot\mathbf{r}} \psi_{n_h}^*(\mathbf{s}) \psi_{n_p}(\mathbf{r} - \mathbf{s}), \quad (27)$$

$$h_p^2 = i\psi_{n_h}^*(\mathbf{s}) [J_{p-1}(|\alpha_l|) e^{-i(p-1)\boldsymbol{\kappa}\cdot\mathbf{r}} \mathcal{V}_{n_p}^+(\mathbf{r} - \mathbf{s}) - J_{p+1}(|\alpha_l|) e^{-i(p+1)\boldsymbol{\kappa}\cdot\mathbf{r}} \mathcal{V}_{n_p}^-(\mathbf{r} - \mathbf{s})], \quad (28)$$

$$h_p^3 = i [J_{p+1}(|\alpha_l|) e^{-i(p+1)\boldsymbol{\kappa}\cdot\mathbf{r}} \mathcal{V}_{n_h}^{+*}(\mathbf{s}) - J_{p-1}(|\alpha_l|) e^{-i(p-1)\boldsymbol{\kappa}\cdot\mathbf{r}} \mathcal{V}_{n_h}^{-*}(\mathbf{s})] \psi_{n_p}(\mathbf{r} - \mathbf{s}). \quad (29)$$

More details concerning the computation of the above expressions are given in Appendix B. The differential cross section for given magnetic quantum numbers of the atoms can be derived from the Fermi golden rule [14,30]

$$d\sigma_{m_p, m_h}^{\text{CBA}} = (2\pi)^4 v^{-1} \sum_{p=-\infty}^{\infty} \left| \sum_{j=1}^3 \mathcal{T}_{m_p, m_h}^j(\mathbf{k}_\beta) \right|^2 \times \delta(\gamma_0 + \langle U \rangle + p\omega_0) d\mathbf{k}_\beta, \quad (30)$$

where $d\mathbf{k}_\beta$ is the infinitesimal component in momentum space. Using the spherical coordinates $(k_\beta, \theta, \varphi)$ for the representation of the \mathbf{k}_β vector, one has

$$d\mathbf{k}_\beta = k_\beta d(k_\beta^2/2) d\hat{\mathbf{k}}_\beta,$$

with the solid angle $d\hat{\mathbf{k}}_\beta = \sin\theta d\theta d\varphi$. Finally, the total cross section is obtained by summing over the final states of \bar{H} , averaging over the initial states of Ps, and performing the integration over $d\mathbf{k}_\beta$, which leads to

$$\sigma^{\text{CBA}} = \frac{(2\pi)^4}{v\hat{l}_p} \sum_{p=-\infty}^{\infty} k_\beta(p) \int_{\Omega} d\hat{\mathbf{k}}_\beta \sum_{m_p, m_h} |\mathcal{T}_{m_p, m_h}^{\text{CBA}}(\mathbf{k}_\beta)|^2 \quad (31)$$

$$\equiv \sum_{p=-\infty}^{\infty} \sigma_p, \quad (32)$$

where $\hat{l}_p \equiv 2l_p + 1$. It is worth mentioning that since both antihydrogen and positronium atoms are composed of a single positron, there is no need to include the spin degree of freedom in Eq. (31). The orientation of $\boldsymbol{\kappa} \parallel \boldsymbol{\mathcal{E}}_0$ regardless of the choice of the scattering geometry implies that $|\mathcal{T}_{m_p, m_h}^j(\mathbf{k}_\beta)|$ are φ independent. The angular θ dependence of these components is then contained in the two coefficients α_l and κ defined by $\alpha_l(\theta, p) = \mathcal{E}_0 k_\beta(p) \cos\theta/\omega_0^2$ and $\kappa(\theta, p) = \omega_0/k_\beta(p) \cos\theta$, respectively.

Since the norm of the final momentum in Eq. (31) is fixed by the δ function in Eq. (30), we also note that the number of photons in the case of net absorption ($p < 0$) by the electron-atom system can be arbitrarily large. In contrast, the decrease of the electron momentum in the case of photon emission ($p > 0$) should be limited by the condition $k_\beta(p) \geq 0$, which implies that $p \leq \lfloor \omega_0^{-1}(v^2 + \epsilon_{n_p} - \epsilon_{n_h} - \langle U \rangle) \rfloor$ for all relevant contributions of positive order involved in the cross-section calculation. Moreover, since the laser-atom coupling is taken into account to lowest order in the field, the widths

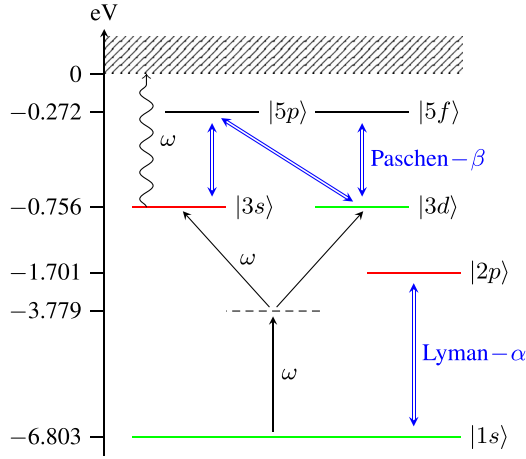


FIG. 2. Energy-level diagram of Ps. Light green straight lines represent states produced within the framework of the GBAR experiment, red straight lines states not produced, and double blue lines virtual transitions involved in the laser-assisted reaction.

of the atomic levels cannot be introduced consistently. As a result, our model is not valid at resonance [31]. Nevertheless, our model provides useful information about the behavior of the cross section in the vicinity of the resonance. The values of laser detuning and field strength in the perturbative regime are discussed later according to experimental constraints for the GBAR experiment.

III. RESULTS AND DISCUSSION

Since the calculations are very time consuming, we have parallelized our program written in FORTRAN 95. The parallelization has been performed using the message passing interface on the variables (p, θ) involved in Eq. (31). The computation of the numerous integrals is performed by using the method of Gaussian quadrature with a number of integration points varying between 32 and 96. In order to achieve the convergence of the scattering amplitude, the required number of partial waves (see l , l_f , and l_c in Appendix B) varies between 16 and 24 as a function of the atomic states $\text{Ps}(n_p, l_p)$ and $\bar{\text{H}}(n_h, l_h)$ and the antiproton impact energies.

One of the key issues of the present study is the positronium states involved in the reaction with or without the presence of an external laser. In the following the different positronium states produced (or not) within the framework of the GBAR experiment are discussed (see Fig. 2). A detailed and recent account of the experimental progress in positronium physics can be found in the review in [32]. Positronium is a system consisting of an electron and its antiparticle, a positron. The system is unstable. Depending on the relative spin states, the two particles annihilate each other into two or three γ rays.

(i) *State Ps(1s)*. The ortho-positronium $o\text{-Ps}(1s)$, whose annihilation lifetime is 142 ns, is the only state of Ps produced in the absence of any laser source. It is produced via the capture of an electron by a positron and resulting from the bombardment of a positron beam on a nanoporous silica plate situated in a tube forming the collision cell.

(ii) *State Ps(2p)*. The production of $\text{Ps}(2p)$ requiring the use of a UV-C laser source with wavelength of 243 nm is currently improbable since the laser-repetition period available for the GBAR experiment is 13 ns. Indeed, the latter is almost more than three times larger than the radiative lifetime of this state, equal to 3.2 ns. Furthermore, as described later, the first-order Doppler effect is also a major obstacle to the production of the $2p$ state. This is the reason why we present only the cross sections for $\text{Ps}(2p)$ in the zero-field case.

(iii) *State Ps(3d)*. The production of $\text{Ps}(3d)$ (having a radiative lifetime of 31 ns) is obtained from the ground state via a two-photon transition (see Fig. 2) of frequency $\omega = 3.024$ eV (410 nm). The process is performed by using two counterpropagating Ti:sapphire laser beams that are doubled in frequency in order to compensate for the first-order Doppler effect [4].

(iv) *State Ps(3s)*. This state cannot be produced using the protocol employed for $\text{Ps}(3d)$. Indeed, the probability that $\text{Ps}(3s)$ will be photoionized by the absorption of a supplementary photon is much higher compared to the same process for $\text{Ps}(3d)$. This is due to the fact that in the experimental configuration used for $\text{Ps}(3d)$, the photoionization probability for $\text{Ps}(3s)$ is of the order of 63%, compared to 5% for $\text{Ps}(3d)$ (details of the calculation are available in [4,20]). However, $\text{Ps}(3s)$ constitutes an interesting candidate because of its long radiative lifetime of 320 ns and its coupling with the external field. In addition, three-body reaction cross sections may be computed with much less computational effort due to the s ($l_p = 0$) character of this Ps state.

In what follows, the cross sections are given in units of $\pi a_0^2 = 0.88 \times 10^{-16}$ cm² as a function of the antiproton impact energy.

A. Zero-field case

According to the considerations above, we start by presenting the zero-field partial cross sections for $\text{Ps}(3d)$ in Fig. 3, which have been obtained by summing cross sections of reaction (a) with the same principal quantum number n_h from $n_h = 2$ up to $n_h = 7$. They have been calculated in the CBA formalism by considering the prior form of the \mathcal{S} -matrix elements. In comparison with the CBA cross sections computed in the post form by Comini *et al.* for $n_h = 2$, the convergence of our calculations has been verified, as long as there is no post-prior discrepancy in the absence of a laser field. Nevertheless, since the states of the produced $\bar{\text{H}}$ are generally not measured experimentally, one must consider the so-called inclusive cross section defined by

$$\text{Ps}(n_p, l_p) + \bar{p} \rightarrow \sum_{n_h=1}^{\sup n_h} \sum_{l_h=0}^{n_h-1} \bar{\text{H}}(n_h, l_h) + e^- \quad (33)$$

These cross sections with Ps in different initial states (n_p, l_p) are depicted in Fig. 4. It is important to mention that the inclusive cross section associated with $\text{Ps}(1s)$ differs from those associated with the excited states of Ps, for which all output channels are open at 1 keV. In particular, only the $\bar{\text{H}}(1s)$ channel is open at 1 keV, followed by the contribution of the $\bar{\text{H}}(2s + 2p)$ channels above 3.12 keV and the $\bar{\text{H}}(3s + 3p + 3d)$ channels above 4.86 keV. This leads to several jumps in

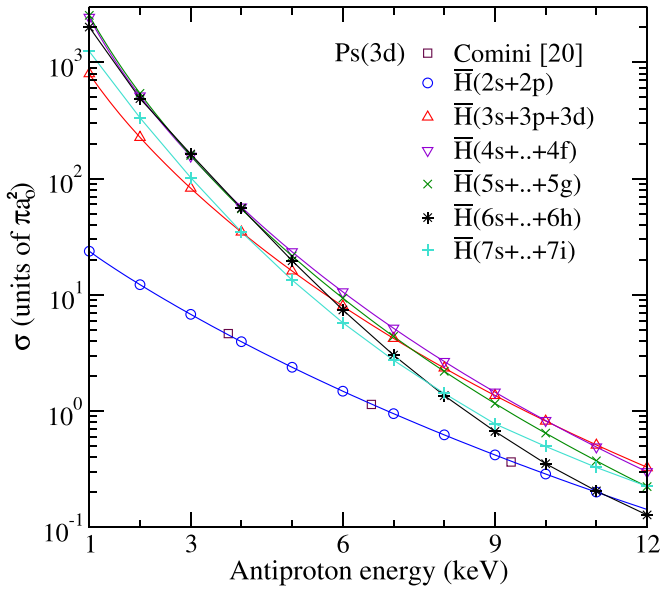


FIG. 3. Antihydrogen production partial cross sections (sum over l_h only) from $\text{Ps}(3d)$ as a function of antiproton impact energy. The CBA cross sections previously computed by Comini [20] for the channels $\bar{\text{H}}(2s+2p)$ are shown. The solid lines serve as guidelines.

the behavior of the $\text{Ps}(1s)$ inclusive cross section. Moreover, we can clearly see that below 7 keV, a preparation of Ps atom $n_p = 3$ states leads to an important increase of the inclusive capture cross sections with respect to the situation with $\text{Ps}(1s)$. The only available experimental data for reaction (a) displayed in Fig. 4 are from the work published by Merrison *et al.* [19]. In this experiment, protons at about 10 keV were sent through a cloud of ground-state positronium and the total

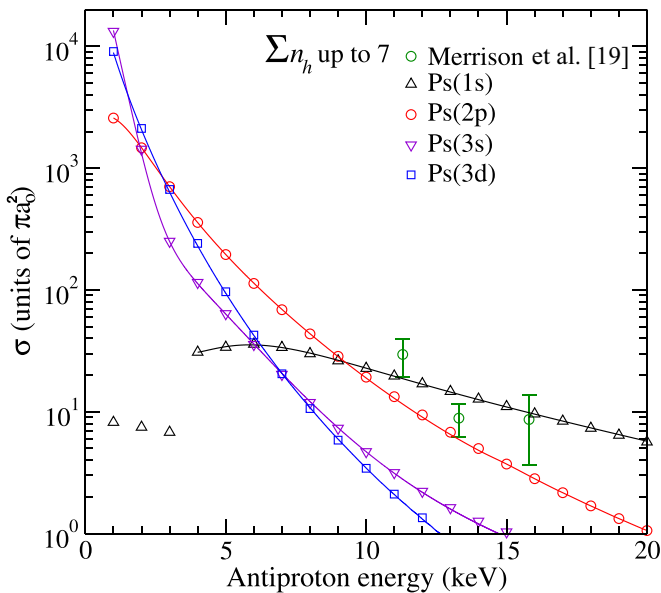


FIG. 4. Inclusive cross sections of antihydrogen production from $\text{Ps}(n_p, l_p)$ up to the state $\bar{\text{H}}(7i)$, as a function of the antiproton impact energy. The three experimental points are due to Merrison *et al.* [19]. The solid lines serve as guidelines.

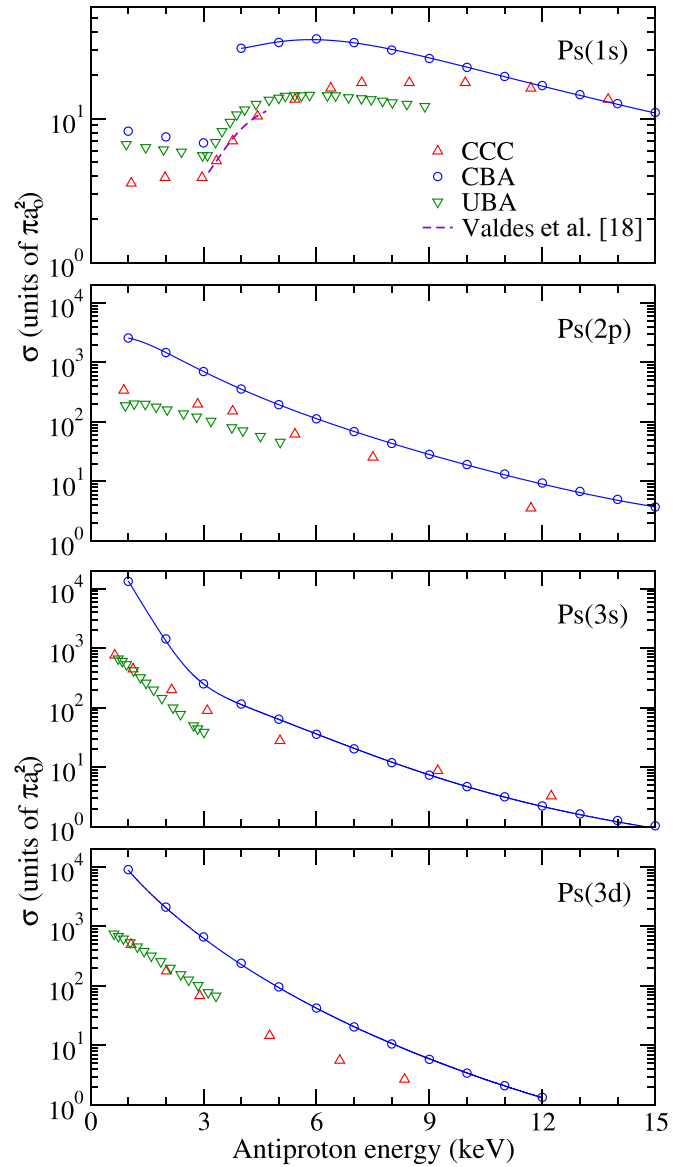


FIG. 5. Inclusive cross sections of antihydrogen production resulting from the CCC [8], UBA [33,34] [up to the state $\bar{\text{H}}(7i)$], and present CBA [up to the state $\bar{\text{H}}(7i)$] calculations, for a specific state of Ps , as a function of the antiproton impact energy. The dashed lines for $\text{Ps}(1s)$ cross sections, resulting from the resolution of the Faddeev-Merkuriev equations, are due to Valdes *et al.* [11]. The solid lines serve as guidelines.

hydrogen production cross section was measured based on the detection of the escaping free positron.

In Fig. 5 we compare our CBA inclusive cross sections with those obtained from the two-center close-coupling convergent (CCC) method and the unitarized Born approximation (UBA) [33,34]. Although the CBA cross sections remain higher than the CCC cross sections at antiproton energies up to 10 keV, the obtained results show that the Coulomb Born approximation is strengthened as the impact energy increases. At low antiproton energies (around 1 keV), the CCC and CBA cross sections related to $\text{Ps}(3s, 3d)$ differ approximately by an order of magnitude (approximately

$10\pi a_0^2$). However, the results of the *ab initio* calculations based on the Faddeev-Merkuriev equations [11,35] for the reaction $\text{Ps}(1s) + \bar{p} \rightarrow \bar{\text{H}}(2s + 2p) + e^-$ are in very good agreement with those of the CCC calculations. The latter are depicted for antiproton energies ranging from 3.12 to 4.86 keV (see the discussion above). Moreover, only CBA cross sections computed with $\text{Ps}(1s)$ and $\text{Ps}(3s)$ seem to agree with CCC cross sections for antiproton energies greater than 6 and 8 keV, respectively. In contrast, the UBA cross sections are closer to the CCC cross sections. This is because at low antiproton energies, the UBA formalism describes the collision more appropriately than the CBA formalism. Indeed, it consists in a modification of the Born series [36], which allows one to extend the range in energy over which the development of the first order remains valid.

B. Cross sections with $\text{Ps}(1s)$ in the presence of an external laser field

One of the most efficient ways to produce a gas made of positronium is to irradiate a nanoporous material with a highly energetic positron beam. The positrons lose their initial kinetic energies by collisions with the atoms of the solid and the positronium is formed by capturing one electron from one orbital state of the solid. In the case of nanoporous materials, the positronium is mostly formed in the proximity to the internal surfaces of the pores and diffuses inside the solid until it escapes into the vacuum. Various experiments [37] have established that when the positronium is prepared by using nanoporous materials such as silica, depending on the size of the pores, the atoms are emitted either with an energy corresponding to the temperature of the solid (usually the room temperature associated with an average thermal energy of 25 meV) or with an energy significantly higher (typically around 48 meV). Indeed, for small nanopores ($d \geq 5.5$ nm [38]) the bound energy of positronium inside the pore [which can be estimated using $(\hbar\pi)^2/m_e d^2$] exceeds the thermal energy leading to a higher escaping energy. In the setup of the GBAR experiment, a diameter of $d = 3\text{--}4$ nm leads to $\langle E_{\text{Ps}} \rangle = 48$ meV, where $\langle E_{\text{Ps}} \rangle$ is the confinement energy of Ps atom. In the following we will consider these two physical situations and assume that positronium atoms thermalize quasi-instantaneously inside the pore to a Maxwell-Boltzmann distribution [39,40]. From the above discussion, one deduces the full width at half maximum of the broadening of spectral lines due to the Doppler effect [41]

$$\Delta\nu_D = \frac{v_0}{c} \sqrt{8\langle E_{\text{Ps}} \rangle \ln 2/m_{\text{Ps}}}, \quad (34)$$

where $v_0 = \omega_0/2\pi$ is the frequency of the emitting source. Let us start by considering the case of 25 meV confinement energy. Using Eq. (34) and considering a laser frequency $v_0 \sim v_{21} = 1233$ THz in the vicinity of the Lyman- α transition, we obtain that $\Delta\nu_D = 454.3$ GHz. This value can be compared to the experimental value of 672 ± 43 GHz obtained by Deller *et al.* [38], suggesting the use of a laser source with a large spectral width. Therefore, we propose to consider the laser sources given in the following. These laser sources

have a large pulse duration according to the considerations made in Sec. II.

The laser source L_1 that can be built at CERN is a Fourier-transform-limited laser pulse. It has an energy per pulse of $E_\tau = 10 \mu\text{J}$, a beam spot size of $w_0 = 0.5$ mm, and a pulse duration of $\tau = 2$ ps. It leads to a spectral width of $\Delta\nu_0 = 0.441/\tau = 220.5$ GHz in the case of a Gaussian beam profile and a peak intensity of $I_{\text{cr}} = E_\tau/\pi w_0^2 \tau = 6.37 \times 10^8$ W/cm² (i.e., an electric-field strength of $\mathcal{E}_{\text{cr}} = 6.93 \times 10^5$ V/cm). The main inconvenient of this source is that its pulse duration is very short compared to the interaction time (time for which an antiproton of the incident beam is likely to interact with a positronium atom contained in the tubular cell) given by $t_{\text{int}} = l/v_{\bar{p}}$, where $v_{\bar{p}} = \sqrt{2E_{\bar{p}}/m_{\bar{p}}}$ is the antiproton velocity. Indeed, if one considers a collision cell of length $l = 20$ mm [5], we obtain that $t_{\text{int}} = 13\text{--}46$ ns for an antiproton energy range from 1 to 12 keV.

The chirped pulse laser source L_2 was proposed by Deller *et al.* This later presents the advantage of having a spectral width $\Delta\nu_0 = 225 \pm 3$ GHz similar to a Fourier-transform-limited laser source L_1 , with a pulse duration of $\tau = 8 \pm 1$ ns. The energy per pulse of this laser is $E_\tau = 1.2 \pm 0.3$ mJ and the peak intensity for the same spot size as for L_1 is $I_{\text{cr}} = 1.91 \times 10^7$ W/cm² (i.e., an electric-field strength of $\mathcal{E}_{\text{cr}} = 1.22 \times 10^5$ V/cm).

First of all, in order to obtain an appreciable density of photons in the vicinity of the resonance, we will consider in the following and for the two types of lasers a frequency detuning $\Delta\nu = \frac{1}{2}\Delta\nu_0 \sim -110$ GHz, where $\Delta\nu \equiv \nu_0 - \nu_{21}$. This frequency detuning implies that the natural width $\Gamma_{\text{rad}}(2p)$ of the final state $2p$ may be neglected for the cross-section computation. Indeed, we have $\Delta\nu \gg \Gamma_{\text{rad}}(2p) = 0.313$ GHz and therefore it is not necessary to add an imaginary component at the energies involved in the Coulomb Green's operator.

Second, in order to justify the use of a first-order perturbation theory for modeling the positronium-laser interaction, the value of \mathcal{E}_0 is chosen such that the transition probability obtained from the projection of the initial state (8) on the state $|2p\rangle$ remains smaller than unity, namely,

$$\Omega_1 < |\Delta\omega|, \quad (35)$$

where $\Omega_1 = |\langle 2p|\mathcal{E}_0 \cdot \mathbf{r}|1s\rangle|$ corresponds to the Rabi frequency. From the considerations above, we subsequently consider $\mathcal{E}_0 \leq 5 \times 10^4$ V/cm $< \mathcal{E}_{\text{cr}}$ for the source L_1 (i.e. $\Delta\nu = -110.25$ GHz), which leads to $(\Omega_1/\Delta\omega)^2 \leq 0.747$, in agreement with (35), where $\Omega_1 \leq 2\pi \times 95.32$ GHz.

Furthermore, as the electric-field strength that we consider leads to a very small value of the electron-field coupling parameter ($|\alpha_l|_{p=0} \leq 4 \times 10^{-4}$ below 20 keV of antiproton energy), the dressed states of the electron do not contribute significantly to the calculation of σ^{CBA} [42]. In other words, the behavior of Bessel functions in the vicinity of the origin implies that for $p = 0$ the term \mathcal{F}_0^1 (27) is dominant among the other matrix elements \mathcal{F} . It leads to $\sigma_0 \sim \sigma^{\text{CBA}}(\mathcal{E}_0 = 0)$ in Eq. (32), for which the convergence is obtained by limiting the summation to $|p| \leq 1$. Furthermore, by isolating in \mathcal{F}_p^2 the resonant term $G_c(\epsilon_{n_p} + \omega_0)$ multiplied by J_{p+1} [see Eq. (28)], one notices that the process of one-photon

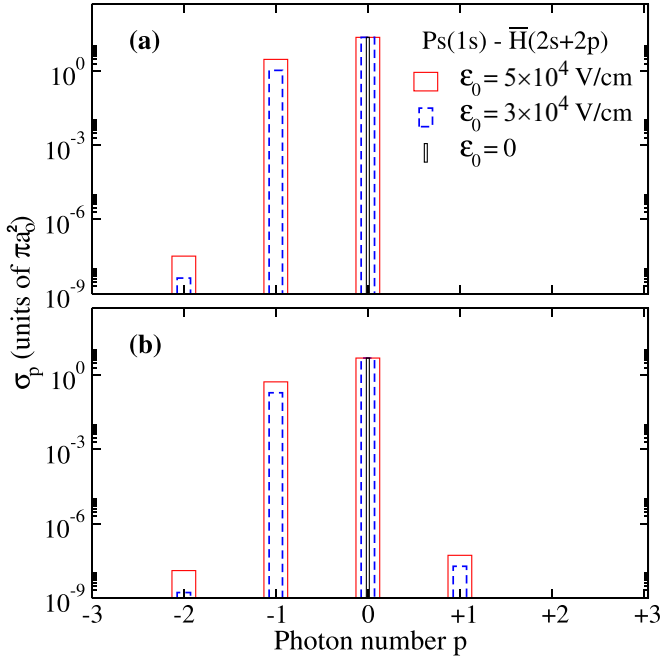


FIG. 6. Antihydrogen production partial cross sections involving the exchange of p photons, for the output channels $\bar{H}(2s+2p)$ and different values of the electric-field strength. The antiproton impacting energy is (a) 6 keV and (b) 15 keV.

absorption ($p = -1$) is dominant with respect to the process of one-photon emission ($p = +1$). This leads us to consider that

$$\sigma^{\text{CBA}} \sim \sigma_0 + \sigma_{-1}. \quad (36)$$

This behavior is illustrated in Fig. 6, where the partial cross sections $\bar{p} + \text{Ps}(1s) \rightarrow \bar{H}(2s+2p) + e^-$ involving the exchange of p photons [see Eq. (32)] are depicted for two incident antiproton energies. The choice of these particular output channels is justified by the fact that the species $\bar{H}(2s)$ and $\bar{H}(2p)$ have the highest contributions for the production of \bar{H} via reaction (a). The corresponding partial CBA cross section obtained by summing the contributions σ_p in Eq. (36) is depicted in Fig. 7.

In Fig. 8(a) we represent the gain produced by the presence of the laser on the inclusive cross sections. This is done for a laser frequency detuning of $\Delta\nu = -110.25$ GHz. Close to 6 keV where the cross section is maximum our model predicts an increase of 18.9% for the source L_1 ($\mathcal{E}_0 = 5 \times 10^4$ V/cm) and 27% for the source L_2 ($\mathcal{E}_0 = 5.8 \times 10^4$ V/cm). The latter simulation corresponds to the limit of validity of our model with $(\Omega_1/\Delta\omega)^2 = 0.966$. Moreover, the role played by the Doppler effect on the inclusive cross section is also investigated in Fig. 8(b). In order to do so we use the values for the frequency detunings

$$\Delta\nu := \Delta\nu + \frac{1}{2}\Delta\nu_D = 116.9 \text{ GHz}, \quad (37)$$

$$\Delta\nu := \Delta\nu - \frac{1}{2}\Delta\nu_D = -337.4 \text{ GHz}, \quad (38)$$

where $\Delta\nu_D = 454.3$ GHz is the Doppler broadening width previously obtained from Eq. (34) for $\langle E_{\text{Ps}} \rangle = 25$ meV. As expected, for $\Delta\nu = 116.9$ GHz (37) we find almost the same

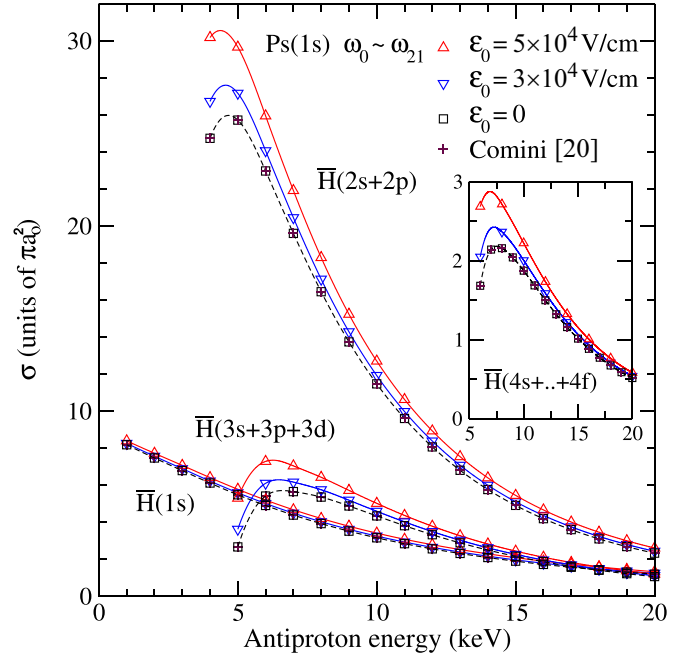


FIG. 7. Antihydrogen production partial cross sections as a function of the impacting antiproton energy, for different values of the laser electric field \mathcal{E}_0 . The zero-field CBA cross sections previously computed by Comini [20] for the channels $\bar{H}(1s)$ and $\bar{H}(2s+2p)$ are shown. The dashed and solid lines serve as guidelines.

results already obtained for $\Delta\nu = -110.25$ GHz. This is due to the fact that these two values are symmetrically distributed with respect to the resonance situation (zero detuning). However, for $\Delta\nu = -337.4$ GHz (38), the situation is completely different. This is because we are much further from resonance where the photon density is small. The consequence is a decrease of the cross section which is almost identical to the one without the external field. Thus, a future investigation at $\langle E_{\text{Ps}} \rangle = 48$ meV for $\text{Ps}(1s)$ with the same laser parameters will not lead to higher cross sections far away from the resonance.

C. Cross sections for $\text{Ps}(3s)$ and $\text{Ps}(3d)$ in the presence of a laser field

Since the use of a chirped pulse laser which verified $|\Delta\nu| \gg \frac{1}{2}\Delta\nu_D$ seems to be the best theoretical and experimental compromise given the investigations made for $\text{Ps}(1s)$, we will consider an IR-B laser having a wavelength around 2563 nm with the same detuning as before (i.e., $\Delta\nu = -110.25$ GHz) for the investigation of $\text{Ps}(n_p = 3)$. This leads to consider a laser frequency located near the Paschen- β line, as we can see in Fig. 2. Such a laser source can be adapted from laser L_2 (described in [38]), which use an optical parametric oscillator. The advantage considering this source is to get a full overlap of the Doppler broadening width at Ps confinement energies of 25 meV ($\Delta\nu_D = 43.04$ GHz) and 48 meV ($\Delta\nu_D = 59.64$ GHz). In this section we will also investigate the more realistic case of $\langle E_{\text{Ps}} \rangle = 48$ meV [see the discussion in Sec. III B above Eq. (34)].

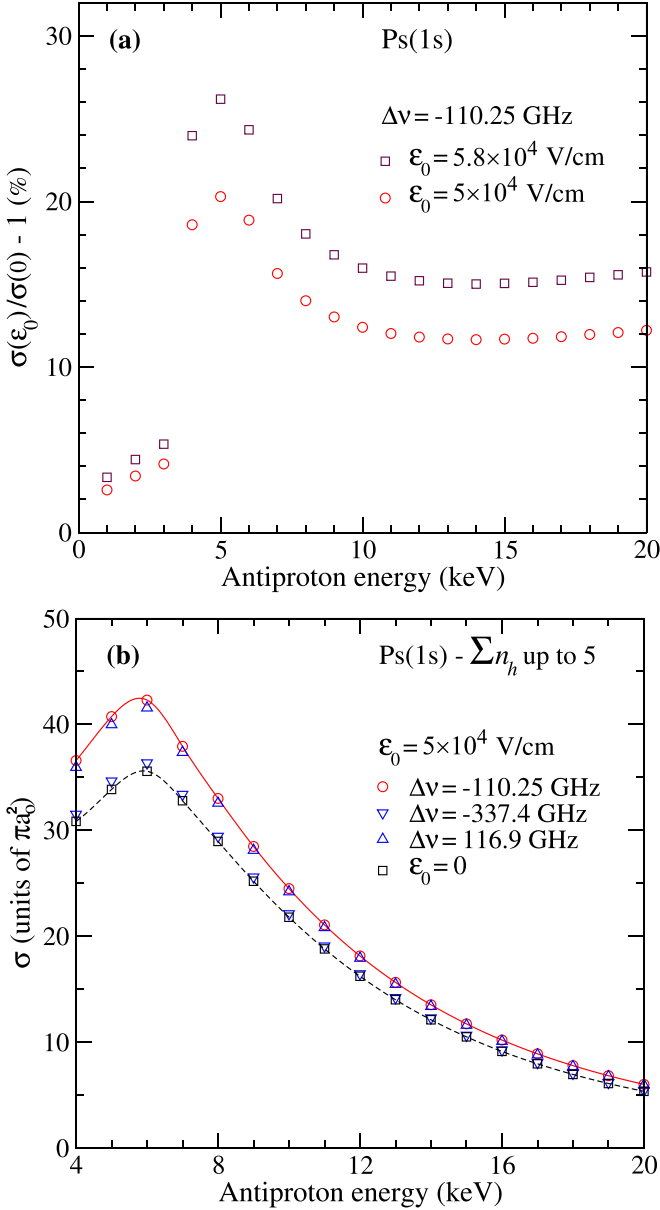


FIG. 8. (a) Relative increase in percentage and with respect to the zero-field situation of the inclusive cross section for two values of the laser electric field. (b) Inclusive cross sections for $\epsilon_0 = 0$ (without Doppler broadening), $\epsilon_0 = 5 \times 10^4$ V/cm and $\Delta\nu = -110.25$ GHz (with Doppler broadening), and $\Delta\nu_D = 454.3$ GHz leading to $\Delta\nu = -337.4$ GHz and $\Delta\nu = 116.9$ GHz. The dashed and solid lines serve as guidelines.

For Ps(3s) let us first consider the $3s$ - $5p$ transition. We check that the width of the spectral line associated with the radiative relaxation of the final state $\Gamma_{\text{rad}}(5p) = 21.46$ MHz remains negligible in front of the laser detuning. With respect to the case of Ps(1s), we consider here a smaller electric-field strength $\epsilon_0 = 2.5 \times 10^4$ V/cm, which should lead to larger changes of the cross sections. This is due to the fact that since the $3s$ state is less bound than $1s$, it must be more sensitive to the presence of an external perturbation. The corresponding coupling constant is $(\Omega_1/\Delta\omega)^2 = 0.573$, with $\Omega_1 = 2\pi \times 83.46$ GHz.

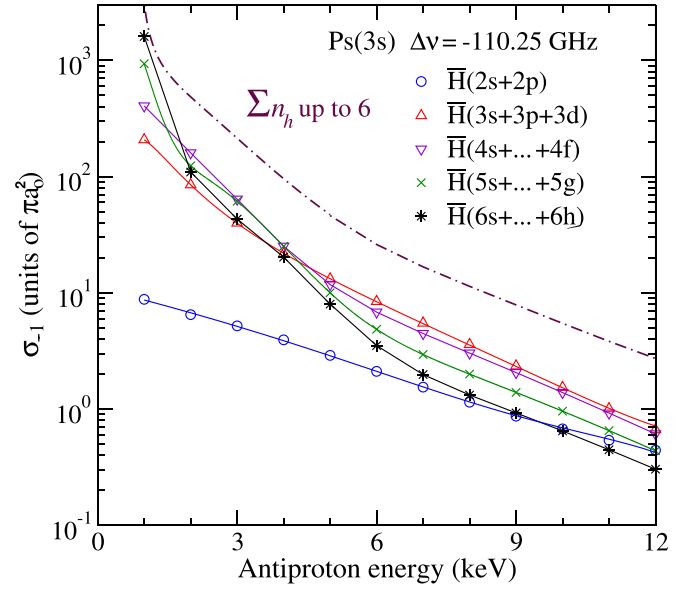


FIG. 9. Antihydrogen production partial cross sections from Ps(3s) due to the one-photon absorption by the system, as a function of antiproton impact energy $\epsilon_0 = 2.5 \times 10^4$ V/cm and $\Delta\nu = -110.25$ GHz. The dashed and solid lines serve as guidelines.

In Fig. 9 partial cross sections σ_{-1} (summed over l_h only) due to the absorption of one photon [see Eq. (36)] are depicted for the ideal situation without Doppler broadening ($\Delta\nu_D = 0$). Inclusive cross sections are shown in Fig. 10. Different laser detuning are considered depending on the mean energy of Ps when the Doppler broadening is considered (see Table I). At 2 keV of antiproton energy where the zero-field inclusive cross section take on substantial values, we observe that our

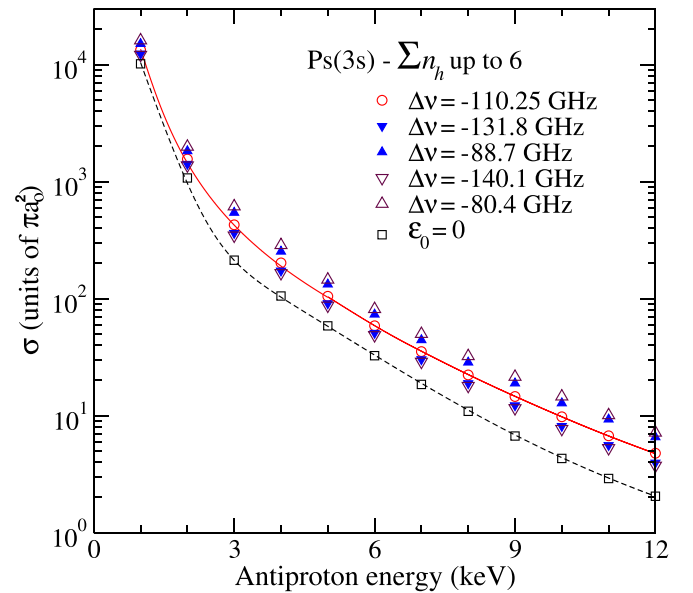


FIG. 10. Inclusive cross sections for $\epsilon_0 = 0$ (without Doppler broadening) and $\epsilon_0 = 2.5 \times 10^4$ V/cm and $\Delta\nu = -110.25$ GHz (with Doppler broadening), with $\Delta\nu_D = 43$ GHz (blue triangles) and $\Delta\nu_D = 59.6$ GHz (brown triangles). The dashed and solid lines serve as guidelines.

TABLE I. Laser detunings and corresponding coupling parameters for $\mathcal{E}_0 = 2.5 \times 10^4$ V/cm as a function of the Ps confinement energy (the initial value of laser detuning when $\langle E_{\text{Ps}} \rangle = 0$ is $\Delta\nu = -110.25$ GHz).

$\langle E_{\text{Ps}} \rangle$ (meV)	$\Delta\nu_{\text{D}}$ (GHz)	$\Delta\nu$ (GHz)	$(\Omega_1/\Delta\omega)^2$
25	43.04	min -131.8	0.401
25	43.04	max -88.7	0.885
48	59.64	min -140.1	0.355
48	59.64	max -80.4	1.077

model predicts an increase (with respect to the zero-field situation) of the inclusive cross section depending on the laser detuning. This increase is of the order of 61.1% for $\langle E_{\text{Ps}} \rangle = 0$, at least 46.1% for $\langle E_{\text{Ps}} \rangle = 25$ meV, and at least 42% for $\langle E_{\text{Ps}} \rangle = 48$ meV. For the sake of clarity, the predictions for higher antiproton energies and/or as close as possible to resonance are given in Table II.

For Ps($3d$) let us now consider the $3d$ -($n_p = 5$) transition using the same laser parameters as for Ps($3s$). Since the width of the spectral line associated with the radiative relaxation of the final state $5f$ is 3.57 MHz, the condition $\Delta\nu = -110.25$ GHz \gg ($\Gamma_{\text{rad}}(5p)$, $\Gamma_{\text{rad}}(5f)$) is still valid. Moreover, the value of the transition probability obtained for the parameters $\mathcal{E}_0 = 2.5 \times 10^4$ V/cm and $\langle E_{\text{Ps}} \rangle = 0$ (leading to $\Omega_1 = 2\pi \times 95.62$ GHz) is $(\Omega_1/\Delta\omega)^2 = 0.752$. We observe that the coupling of the initial state $3d$ to the final state $5f$ (associated with an orbital $l_p + 1$) is more favorable than to the state $5p$ (associated with $l_p - 1$). Indeed, the Rabi frequency is expressed as

$$\Omega_1 = 2\pi\mathcal{E}_0\sqrt{(\Omega_1^{(l_p-1)})^2 + (\Omega_1^{(l_p+1)})^2}, \quad (39)$$

$$\Omega_1^{(l_p-1)} \equiv |\langle 5p|\hat{\mathbf{z}} \cdot \mathbf{r}|3d\rangle| = 4.51 \times 10^{-4} \text{ Hz cm/V}, \quad (40)$$

$$\Omega_1^{(l_p+1)} \equiv |\langle 5f|\hat{\mathbf{z}} \cdot \mathbf{r}|3d\rangle| = 3.80 \times 10^{-3} \text{ Hz cm/V}, \quad (41)$$

which implies that $\Omega_1^{(l_p-1)} \sim 0.12\Omega_1^{(l_p+1)}$.

In Fig. 11 partial cross sections σ_{-1} are depicted without Doppler broadening ($\Delta\nu_{\text{D}} = 0$). As before, the inclusive cross sections are also shown in Fig. 12. However, since the Rabi frequency is slightly higher than the one of Ps($3s$), the condition (35) is not satisfied as close as possible to resonance, i.e., for $\Delta\nu := (-88.7$ GHz, -80.4 GHz), and since the convergence of σ_{-1} for the channel $\bar{\text{H}}(n_h = 6)$ is not obtained at 12 keV, the inclusive cross sections are shown for antiproton energy up to 10 keV.

At 2 keV of antiproton energy, our model predicts an increase of the zero-field inclusive cross section of the order of 17.6% for $\langle E_{\text{Ps}} \rangle = 0$, at least 12.3% for $\langle E_{\text{Ps}} \rangle = 25$ meV, and at least 10.7% for $\langle E_{\text{Ps}} \rangle = 48$ meV (see Table II for the other estimates). These increases are smaller to those obtained for Ps($3s$).

Finally, the inclusive gains for Ps($3s$) and Ps($3d$) are represented in Fig. 13. They have been obtained for $\langle E_{\text{Ps}} \rangle = 0$ and $\mathcal{E}_0 = 2.5 \times 10^4$ V/cm. It is worth noticing that the influence of the external electric field may increase significantly the production of antihydrogen [more than a factor of 2 for Ps($3s$) and Ps($3d$) at antiproton energies higher than 9 keV].

TABLE II. Inclusive cross sections $\sigma^{\text{CBA}}[\text{Ps}(n_p = 3)]$ and corresponding gains obtained for $\mathcal{E}_0 = 2.5 \times 10^4$ V/cm as functions of the antiproton and Ps confinement energies. For each antiproton energy, the cross-section values are obtained by considering laser detunings given in Fig. 10 for Ps($3s$) and Fig. 12 for Ps($3d$). The numbers in square brackets refer to multiplication by powers of 10.

$E_{\bar{p}}$ (keV)	$\langle E_{\text{Ps}} \rangle$ (meV)	$\sigma(\mathcal{E}_0)$ (πa_0^2)	$\sigma(\mathcal{E}_0)/\sigma(0)$
Ps($3s$)			
4	0	2.01961[2]	1.963
4	25	1.73034[2]	1.682
4	25	2.52618[2]	2.455
4	48	1.65268[2]	1.606
4	48	2.86664[2]	2.786
6	0	5.86088[1]	1.780
6	25	5.08085[1]	1.543
6	25	7.32758[1]	2.225
6	48	4.87143[1]	1.479
6	48	8.14481[1]	2.474
8	0	2.22749[1]	1.997
8	25	1.88705[1]	1.691
8	25	2.84976[1]	2.554
8	48	1.79564[1]	1.609
8	48	3.22424[1]	2.890
10	0	9.77465[0]	2.234
10	25	8.13940[0]	1.860
10	25	1.27748[1]	2.919
10	48	7.70037[0]	1.760
10	48	1.45626 [1]	3.328
Ps($3d$)			
1	0	9.13012[3]	1.194
1	25	8.68561[3]	1.136
1	48	8.56469[3]	1.120
2	0	2.04156[3]	1.176
2	25	1.95009[3]	1.123
2	48	1.92269[3]	1.107
3	0	6.31964[2]	1.183
3	25	6.02748[2]	1.128
3	48	5.94467[2]	1.113
4	0	2.42560[2]	1.242
4	25	2.28450[2]	1.170
4	48	2.24558[2]	1.150
6	0	5.64857[1]	1.537
6	25	5.06263[1]	1.377
6	48	4.90488[1]	1.334
8	0	1.95196[1]	2.054
8	25	1.65307[1]	1.739
8	48	1.57280[1]	1.655
10	0	8.49007[0]	2.775
10	25	6.86887[0]	2.245
10	48	6.43348[0]	2.103

As we can see, we have checked that the results are almost unchanged with an increase in the number of antihydrogen states included in the calculation.

IV. CONCLUSION

In this work we have studied theoretically the possibility to increase the probability to form an antihydrogen atom by

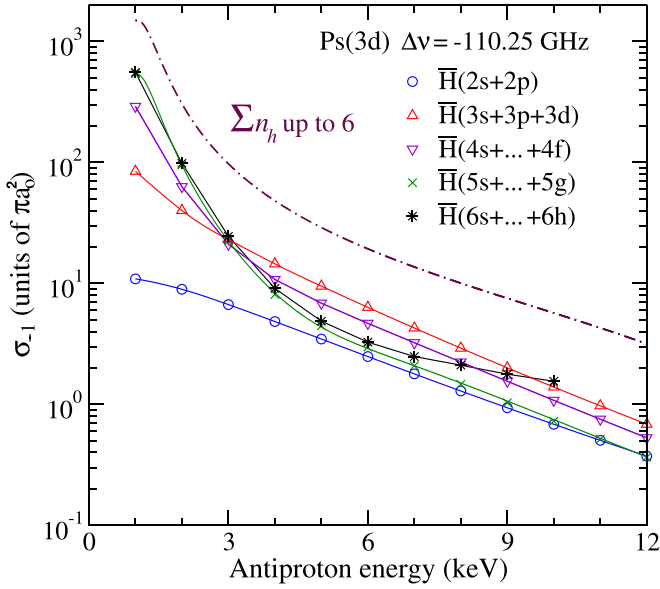


FIG. 11. Antihydrogen production partial cross sections from Ps(3d) due to the one-photon absorption by the system, as a function of antiproton impact energy $\mathcal{E}_0 = 2.5 \times 10^4$ V/cm and $\Delta\nu = -110.25$ GHz. The dashed and solid lines serve as guidelines.

irradiating, with an appropriate laser source, a three-body charge-exchange collision in which an antiproton impacts a positronium atom. For that purpose, a perturbative approach using the Coulomb-Born approximation for modeling the charged-particle collision and a first-order perturbation theory for describing laser-atoms interactions has been employed. In order to find the best irradiation conditions, much effort was devoted to incorporating into the modeling the experimen-

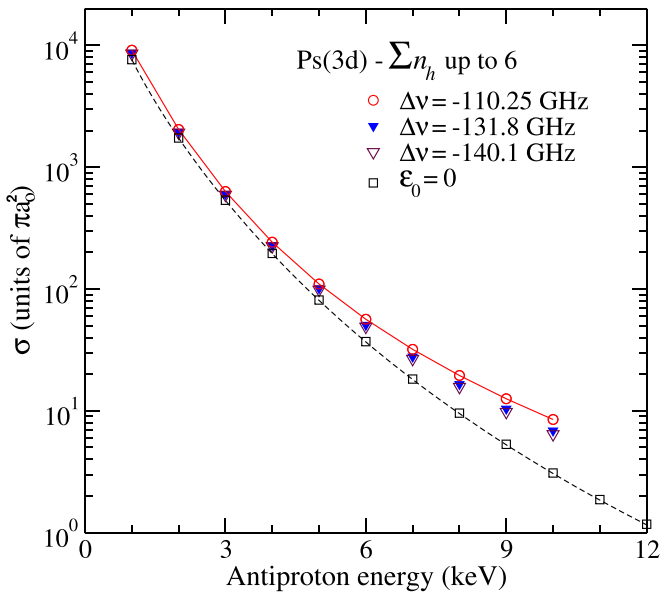


FIG. 12. Inclusive cross sections for $\mathcal{E}_0 = 0$ (without Doppler broadening) and $\mathcal{E}_0 = 2.5 \times 10^4$ V/cm and $\Delta\nu = -110.25$ GHz (with Doppler broadening) with $\Delta\nu_D = 43$ GHz (blue triangles) and $\Delta\nu_D = 59.6$ GHz (brown triangles). The dashed and solid lines serve as guidelines.

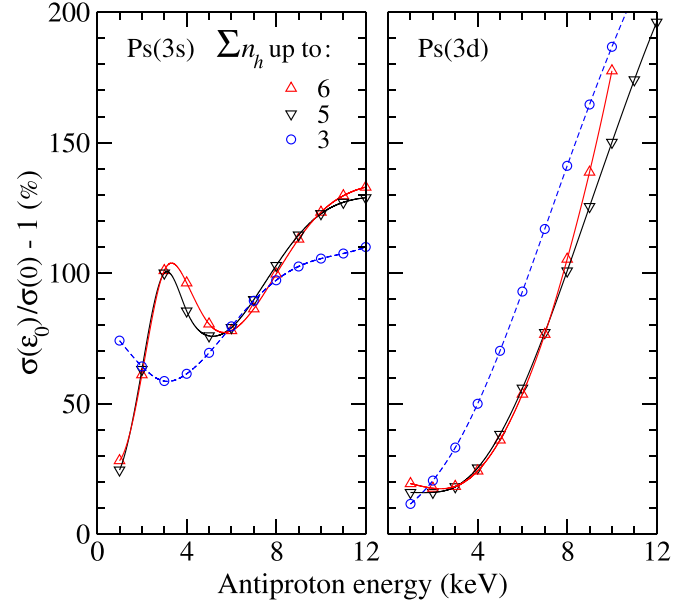


FIG. 13. Inclusive gains for Ps($n_p = 3$) obtained by considering $\mathcal{E}_0 = 2.5 \times 10^4$ V/cm and $\Delta\nu = -110.25$ GHz (without Doppler broadening) by including the first six states of \bar{H} (circles), the first 15 states of \bar{H} (down triangles), and the first 21 states of \bar{H} (up triangles). The dashed and solid lines serve as guidelines.

tal constraints encountered in the GBAR experiment. Laser wavelengths and intensities were carefully chosen to be compatible with the hypothesis of the theoretical approach and to preserve the integrity of the atomic partners involved in the collision.

Three states of Ps(1s; 3s; 3d) were considered. For each of them, possible quasis resonant one-photon transitions leading to optimal irradiation conditions were examined. Furthermore, Doppler broadening due to the Ps velocity was taken into account in the model. By using commercially available laser sources with wavelengths around the Lyman- α and Paschen- β transitions of Ps, we showed that the three-body cross sections can be significantly increased in comparison with the zero-field situation. For antiproton energies corresponding to the maximum cross sections for the zero-field case and without including the Doppler broadening, we found an increase of 18.9% for Ps(1s) (6 keV antiproton energy and a laser intensity of 3.3×10^6 W/cm²) and 19.4% for Ps(3d) (1 keV antiproton energy and a laser intensity of 8.3×10^5 W/cm²). These results were obtained for a laser detuning of $\Delta\nu = -110.25$ GHz. Much more important increases (greater than 200%) can be obtained for higher antiproton energies.

For future work we envisage the use of the same methodology for studying the second reaction (b) of interest for the GBAR experiment, which is a more complex four-body reaction, $\text{Ps}(n_p, l_p) + \bar{H}(n_h, l_h) \rightarrow \bar{H}^+ + e^-$, in which the antihydrogen produced in the first reaction interacts with another positronium to create an antihydrogen ion. It will allow one to determine the production rate of the GBAR experiment according to the model proposed in [20,43].

ACKNOWLEDGMENTS

We thank P. Comini, V. Vénier, F. Catoire, and the members of the Department of Ultrafast Optics and Nanophotonics

at IPCMS for useful discussions. We also acknowledge the High-Performance-Computing Center of the University of Strasbourg. This work was supported by ANR (Grant No. ANR-14-CE33-0008).

APPENDIX A: COMPUTATION OF THE INTEGRAL INVOLVING THE COULOMB GREEN'S OPERATOR

In the position representation, the Coulomb Green's function G_c of energy variable $\Omega_{\mp} \equiv \epsilon_{n_p} \mp \omega_0$ is solution of the operator equation [23]

$$(\Omega_{\mp} - \mathcal{H}_{\alpha}^q)G_c(\Omega_{\mp}, \mathbf{q}, \mathbf{q}') = \delta(\mathbf{q} - \mathbf{q}'), \quad (\text{A1})$$

where the nonrelativistic reduced Coulomb Hamiltonian

$$\mathcal{H}_{\alpha}^q = -(2\mu)^{-1} \Delta_q - \frac{Z}{q} \quad (\text{A2})$$

for the two-body problem is used with $\mu = \frac{1}{2}$ and $Z = 1$ [see Eq. (5)]. In order to compute $v_{n_p}^{\pm}(\mathbf{q})$, a separation of the radial and angular components is performed, which can be expressed in terms of \mathbf{r} and \mathbf{s} vectors in the laboratory frame [6]. Since the Coulomb potential is spherically symmetric, the Coulomb Green's function can be expanded in partial waves

$$G_c(\Omega_{\mp}, \mathbf{q}, \mathbf{q}') = \sum_{lm} g_l(\Omega_{\mp}, q, q') Y_l^{m*}(\hat{\mathbf{q}}) Y_l^m(\hat{\mathbf{q}}'), \quad (\text{A3})$$

where g_l is the radial component of degree l . According to the orientation of the electric field along the z axis, the same operation can be performed in the scalar product on the right-hand side of Eq. (10), which can be written as $\mathcal{E}_0 \cdot \mathbf{q}' = 2(\pi/3)^{1/2} \mathcal{E}_0 q' Y_1^0(\hat{\mathbf{q}}')$. Consequently, the integration of three spherical harmonics of common argument $\hat{\mathbf{q}}'$ gives the $3j$ coefficients, with an angular momentum $\mathcal{L}_p = l_p \pm 1$ for the spherical harmonic function of argument $\hat{\mathbf{q}}$ in Eq. (A3) according to the selection rules for the electric dipole transition $E1$, which has been treated using the development [44]

$$Y_{\mathcal{L}_p}^{m_p}(\hat{\mathbf{q}}) = (-1)^{\mathcal{L}_p+m_p} q^{-\mathcal{L}_p} \sum_{\lambda\mu} (-1)^{\lambda} \sqrt{\hat{\mathcal{L}}_p! \hat{\mathcal{L}}_p! 4\pi [\hat{\lambda}! (\widehat{\mathcal{L}}_p - \lambda)!]^{-1}} r^{\mathcal{L}_p - \lambda} s^{\lambda} \begin{pmatrix} \mathcal{L}_p - \lambda & \lambda & \mathcal{L}_p \\ m_p - \mu & \mu & -m_p \end{pmatrix} Y_{\mathcal{L}_p - \lambda}^{m_p - \mu}(\hat{\mathbf{r}}) Y_{\lambda}^{\mu}(\hat{\mathbf{s}}), \quad (\text{A4})$$

where $0 \leq \lambda \leq \mathcal{L}_p$, $|\mu| \leq \lambda$, and $\hat{\lambda}$ stands for $2\lambda + 1$. In addition,

$$v_{n_p}^{\pm}(\mathbf{r} - \mathbf{s}) = -\frac{1}{2} \mathcal{E}_0 (4\pi \hat{l}_p)^{1/2} \sum_{\mathcal{L}_p} \hat{\mathcal{L}}_p! (\hat{\mathcal{L}}_p!)^{1/2} (-1)^{\mathcal{L}_p} \begin{pmatrix} 1 & l_p & \mathcal{L}_p \\ 0 & 0 & 0 \end{pmatrix} \begin{pmatrix} 1 & l_p & \mathcal{L}_p \\ 0 & m_p & -m_p \end{pmatrix} q^{-\mathcal{L}_p} \mathcal{K}_{n_p \mathcal{L}_p}^{\pm}(q) \\ \times \sum_{\lambda\mu} (-1)^{\lambda} [\hat{\lambda}! (\widehat{\mathcal{L}}_p - \lambda)!]^{-1/2} \begin{pmatrix} \mathcal{L}_p - \lambda & \lambda & \mathcal{L}_p \\ m_p - \mu & \mu & -m_p \end{pmatrix} r^{\mathcal{L}_p - \lambda} s^{\lambda} Y_{\mathcal{L}_p - \lambda}^{m_p - \mu}(\hat{\mathbf{r}}) Y_{\lambda}^{\mu}(\hat{\mathbf{s}}), \quad (\text{A5})$$

$$\mathcal{K}_{n_p \mathcal{L}_p}^{\pm}(q) = \int_{\mathbb{R}_+} dq' q'^3 g_{\mathcal{L}_p}(\Omega_{\mp}, q, q') \mathcal{R}_{n_p l_p}(q'). \quad (\text{A6})$$

Using the projection of the scalar product into the complete basis set of the Legendre polynomial, the radial component of the relation (A5) can be written as

$$V_{\alpha-\beta}(\mathbf{r}, \mathbf{s}) q^{-\mathcal{L}_p} \mathcal{K}_{n_p \mathcal{L}_p}^{\pm}(q) = 4\pi \sum_{lm} \mathcal{J}_{n_p \mathcal{L}_p}^{l, \pm}(r, s) Y_l^{m*}(\hat{\mathbf{r}}) Y_l^m(\hat{\mathbf{s}}), \quad (\text{A7})$$

$$\mathcal{J}_{n_p \mathcal{L}_p}^{l, \pm}(r, s) = \frac{1}{2} \int_{-1}^1 d\xi V_{\alpha-\beta}(\mathbf{r}, \mathbf{s}) q^{-\mathcal{L}_p} \mathcal{K}_{n_p \mathcal{L}_p}^{\pm}(q) P_l(\xi), \quad (\text{A8})$$

where $q = (r^2 + s^2 - 2rs\xi)^{1/2}$ and $V_{\alpha-\beta}$ stands for the prior or post form of the perturbative potential [see the discussion in Sec. II above Eq. (1)]. We note that the perturbative potential is only present in the integrand of Eq. (A8) if the \mathcal{S} -matrix elements are evaluated in the post form. For the evaluation of Eq. (A6), since the spectral representation of $g_{\mathcal{L}_p}$ involves an infinite series which is difficult to compute, we prefer to use the closed-form representation. This representation was first given by Hostler [45] and can be written in terms of regular and irregular Whittaker functions as

$$g_{\mathcal{L}_p}(\Omega_{\mp}, q, q') = -\frac{\beta_{\mp} \Gamma(\mathcal{L}_p + 1 - \beta_{\mp})}{qq'} \frac{M_{\beta_{\mp}, \mathcal{L}_p + 1/2}(2q_{<}/\beta_{\mp}) W_{\beta_{\mp}, \mathcal{L}_p + 1/2}(2q_{>}/\beta_{\mp})}{(2\mathcal{L}_p + 1)!}. \quad (\text{A9})$$

In this relation, $q_{<} = \inf(q, q')$, $q_{>} = \sup(q, q')$, $\beta_{\mp} = \sqrt{\mu}(-2\Omega_{\mp})^{-1/2}$ is the Sommerfeld parameters of the entrance channel, and Γ is the Euler function. Using the expression given in [46], the Whittaker functions of Eq. (A9) can be expressed in terms

of Coulomb radial functions $F_{\mathcal{L}_p}$ (regular) and $G_{\mathcal{L}_p}$ (irregular), which leads to

$$g_{\mathcal{L}_p}(\Omega_{\mp}, q, q') = -2i \frac{\beta_{\mp}}{qq'} F_{\mathcal{L}_p}(-i\beta_{\mp}, -iq_{<}/\beta_{\mp}) H_{\mathcal{L}_p}^{-}(-i\beta_{\mp}, -iq_{>}/\beta_{\mp}), \quad (\text{A10})$$

with $H_{\mathcal{L}_p}^{-} = G_{\mathcal{L}_p} - iF_{\mathcal{L}_p}$. Finally, Eq. (A10) can be computed numerically by using the COULCC subroutine detailed in [47].

APPENDIX B: PARTIAL WAVE EXPANSION OF THE \mathcal{T} -MATRIX ELEMENTS

The equivalent of Eq. (A6) for antihydrogen $\bar{\text{H}}$ is given by

$$\mathcal{K}_{n_h \mathcal{L}_h}^{\pm}(s) = \int_{\mathbb{R}_+} ds' s'^3 g_{\mathcal{L}_h}(\Omega_{\mp}, s, s') R_{n_h l_h}(s'), \quad (\text{B1})$$

where $|l_h - 1| \leq \mathcal{L}_h \leq l_h + 1$ and $\Omega_{\mp} \equiv \epsilon_{n_h} \mp \omega_0$. Using the standard plane-wave expansion [48] and the analytical developments of Appendix A, Eqs. (26)–(29) can be computed using the expressions

$$\mathcal{T}_{p m_p m_h}^j(\mathbf{k}_{\beta}) = (\pi \sqrt{\pi})^{-1} (\hat{l}_p \hat{l}_h)^{1/2} \sum_{l_f} Y_{l_f}^{m_p - m_h}(\hat{\mathbf{k}}_{\beta}) \sum_{(l)_c} i^{l_i + l'_i - l_f - l_c} t_{j(l)_c l_f}^{p m_p m_h}, \quad (\text{B2})$$

$$t_{1(l)_c l_f}^{p m_p m_h} = \sum_{\lambda=0}^{l_p} (\hat{l}_p!)^{1/2} (-1)^{l_p} \mathcal{A}_{(l)\lambda l_c l_f}^{m_p m_h}(l_p, l_h) \mathcal{R}_{1(l)\lambda l_c l_f}^p(l_p, l_h), \quad (\text{B3})$$

$$t_{2(l)_c l_f}^{p m_p m_h} = \frac{i}{2} \mathcal{E}_0 \sum_{\mathcal{L}_p} \hat{\mathcal{L}}_p (\hat{\mathcal{L}}_p!)^{1/2} (-1)^{\mathcal{L}_p + m_p} \begin{pmatrix} 1 & l_p & \mathcal{L}_p \\ 0 & 0 & 0 \end{pmatrix} \begin{pmatrix} 1 & l_p & \mathcal{L}_p \\ 0 & m_p & -m_p \end{pmatrix} \sum_{\lambda=0}^{\mathcal{L}_p} \mathcal{A}_{(l)\lambda l_c l_f}^{m_p m_h}(\mathcal{L}_p, l_h) \mathcal{R}_{2(l)\lambda l_c l_f}^p(\mathcal{L}_p, l_h), \quad (\text{B4})$$

$$t_{3(l)_c l_f}^{p m_p m_h} = \frac{i}{2} \mathcal{E}_0 \sum_{\mathcal{L}_h} \hat{\mathcal{L}}_h (\hat{\mathcal{L}}_h!)^{1/2} (-1)^{l_p + m_h} \begin{pmatrix} 1 & l_h & \mathcal{L}_h \\ 0 & 0 & 0 \end{pmatrix} \begin{pmatrix} 1 & l_h & \mathcal{L}_h \\ 0 & m_h & -m_h \end{pmatrix} \sum_{\lambda=0}^{l_p} \mathcal{A}_{(l)\lambda l_c l_f}^{m_p m_h}(l_p, \mathcal{L}_h) \mathcal{R}_{3(l)\lambda l_c l_f}^p(l_p, \mathcal{L}_h). \quad (\text{B5})$$

In the above expressions, $(l) \equiv (l, l_i, l'_i)$.

Coefficients are derived from the integration over the radial coordinates

$$\mathcal{R}_{j(l)\lambda l_c l_f}^p(l_{\alpha}, l_{\beta}) = \int_{\mathbb{R}_+^2} dr ds r^{l_{\alpha} - \lambda + 2} s^{\lambda + 2} j_l(vr) j_{l_f}(k_{\beta} r) j_{l'_i}(vs) \mathcal{L}_{j l_c}^p(r, s; l_{\alpha}, l_{\beta}), \quad (\text{B6})$$

$$\mathcal{L}_{1 l_c}^p(r, s; l_p, l_h) = J_p(|\alpha_l|) j_{l_c}(p\kappa r) \mathcal{J}_{n_p l_p}^l(r, s) R_{n_h l_h}(s), \quad (\text{B7})$$

$$\mathcal{J}_{n_p l_p}^l(r, s) = \frac{1}{2} \left(\frac{1}{r} - \frac{1}{s} \right) \int_{-1}^1 d\xi q^{-l_p} R_{n_p l_p}(q) P_l(\xi), \quad (\text{B8})$$

$$\mathcal{L}_{2 l_c}^p(r, s; \mathcal{L}_p, l_h) = J_{p+1}(|\alpha_l|) j_{l_c}[(p+1)\kappa r] \mathcal{J}_{n_p \mathcal{L}_p}^{l, -}(r, s) R_{n_h l_h}(s) - (p+1, -) \rightarrow (p-1, +), \quad (\text{B9})$$

$$\mathcal{L}_{3 l_c}^p(r, s; l_p, \mathcal{L}_h) = J_{p-1}(|\alpha_l|) j_{l_c}[(p-1)\kappa r] \mathcal{J}_{n_p l_p}^l(r, s) \mathcal{K}_{n_h \mathcal{L}_h}^{-*}(s) - (p-1, -) \rightarrow (p+1, +). \quad (\text{B10})$$

It should be noted that the rating $(p+1, -) \rightarrow (p-1, +)$ refers to the substitution of the integer $p+1$ and the index $-$ by the integer $p-1$ and the index $+$.

Common coefficients are derived from the integration over the angular coordinates

$$\begin{aligned} \mathcal{A}_{(l)\lambda l_c l_f}^{m_p m_h}(l_{\alpha}, l_{\beta}) &= \frac{(-)^{\lambda} \hat{l}_i \hat{l}'_i \hat{l}_c \hat{l}_f^{1/2}}{\{(2\lambda)! [2(l_{\alpha} - \lambda)]\}^{1/2}} \sum_{(\chi)} \hat{\chi} \hat{\chi}' \hat{\chi}_c \begin{pmatrix} l_f & l_{\alpha} - \lambda & \chi \\ 0 & 0 & 0 \end{pmatrix} \begin{pmatrix} l_c & l & \chi_c \\ 0 & 0 & 0 \end{pmatrix} \begin{pmatrix} l_i & \chi & \chi_c \\ 0 & 0 & 0 \end{pmatrix} \begin{pmatrix} l_{\beta} & \lambda & \chi' \\ 0 & 0 & 0 \end{pmatrix} \\ &\times \begin{pmatrix} l'_i & l & \chi' \\ 0 & 0 & 0 \end{pmatrix} \sum_{\mu} \begin{pmatrix} l_{\alpha} - \lambda & \lambda & l_{\alpha} \\ m_p - \mu & \mu & -m_p \end{pmatrix} \begin{pmatrix} l_f & l_{\alpha} - \lambda & \chi \\ m_h - m_p & m_p - \mu & \mu - m_h \end{pmatrix} \begin{pmatrix} l_c & l & \chi_c \\ 0 & \mu - m_h & m_h - \mu \end{pmatrix} \\ &\times \begin{pmatrix} l_i & \chi & \chi_c \\ 0 & m_h - \mu & \mu - m_h \end{pmatrix} \begin{pmatrix} l_{\beta} & \lambda & \chi' \\ -m_h & \mu & m_h - \mu \end{pmatrix} \begin{pmatrix} l'_i & l & \chi' \\ 0 & m_h - \mu & \mu - m_h \end{pmatrix}. \end{aligned} \quad (\text{B11})$$

Here $(\chi) \equiv (\chi, \chi', \chi_c)$. Using the symmetry properties of the $3j$ coefficients, we have $\sigma_{m_p m_h} = \sigma_{-m_p -m_h}$. This implies that only the evaluation of the terms with $(m_p \leq 0 \cap m_h \leq 0) \cup (m_p > 0 \cap m_h < 0)$ are necessary to obtain the total cross section given in Eq. (31). Note that the upper bounds of three angular moments must be imposed. Arbitrarily, we choose to fix $\sup l$, $\sup l_f$, and $\sup l_c$.

- [1] C. Canali *et al.*, *The AEGIS experiment (Antimatter Experiment: Gravity, Interferometry, Spectroscopy)*, (World Scientific, Singapore, 2010), pp. 185–189, doi: [10.1142/9789814307529_0031](https://doi.org/10.1142/9789814307529_0031).
- [2] M. Doser *et al.* (AEGIS Collaboration), AEGIS (AD-6) status report for 2018, CERN Reports No. CERN-SPSC-2019-007 and No. SPSC-SR-246, 2019 (unpublished).
- [3] S. Eriksson, *Philos. Trans. R. Soc. A* **376**, 20170268 (2018).
- [4] P. Perez *et al.* (GBAR Collaboration), Proposal to measure the gravitational behaviour of antihydrogen at rest, CERN Reports No. CERN-SPSC-2011-029 and No. SPSC-P-342, 2011 (unpublished).
- [5] B. Mansoulié, *Hyperfine Interact.* **240**, 11 (2019).
- [6] P. Comini and P.-A. Hervieux, *New J. Phys.* **15**, 095022 (2013).
- [7] P. Comini, P.-A. Hervieux, and K. Lévêque-Simon, *New J. Phys.* **23**, 029501 (2021).
- [8] A. S. Kadyrov, C. M. Rawlins, A. T. Stelbovics, I. Bray, and M. Charlton, *Phys. Rev. Lett.* **114**, 183201 (2015).
- [9] A. S. Kadyrov, I. Bray, M. Charlton, and I. I. Fabrikant, *Nat. Commun.* **8**, 1544 (2017).
- [10] M. Charlton, Jr., A. P. Mills, and Y. Yamazaki, *J. Phys. B* **50**, 140201 (2017).
- [11] M. Valdes, M. Dufour, R. Lazauskas, and P.-A. Hervieux, *Phys. Rev. A* **97**, 012709 (2018).
- [12] I. I. Fabrikant and H. B. Ambalampitiya, *Phys. Rev. A* **101**, 053401 (2020).
- [13] C. J. Joachain, P. Francken, A. Maquet, P. Martin, and V. Veniard, *Phys. Rev. Lett.* **61**, 165 (1988).
- [14] C. J. Joachain, N. J. Kylstra, and R. M. Potvliege, *Atoms in Intense Laser Fields* (Cambridge University Press, Cambridge, 2011).
- [15] F. W. Byron and C. J. Joachain, *J. Phys. B* **17**, L295 (1984).
- [16] S. Vučić, *Phys. Rev. A* **51**, 4754 (1995).
- [17] E. W. Leonard Mandel, *Optical Coherence and Quantum Optics* (Cambridge University Press, Cambridge, 1995), pp. 504–507.
- [18] O. A. Fojón, R. D. Rivarola, R. Gayet, J. Hanssen, and P. A. Hervieux, *Phys. Rev. A* **54**, 4923 (1996).
- [19] J. P. Merrison, H. Bluhme, J. Chevallier, B. I. Deutch, P. Hvelplund, L. V. Jørgensen, H. Knudsen, M. R. Poulsen, and M. Charlton, *Phys. Rev. Lett.* **78**, 2728 (1997).
- [20] P. Comini, Study of the antihydrogen atom and ion formation in the collisions antiproton-positronium, Ph.D. thesis, Université Pierre et Marie Curie, 2014.
- [21] M. R. C. McDowell and J. P. Coleman, *Am. J. Phys.* **39**, 237 (1971).
- [22] A. B. Voitkiv, B. Najjari, and J. Ullrich, *J. Phys. B* **35**, 2205 (2002).
- [23] A. Maquet, V. Vénier, and T. A. Marian, *J. Phys. B* **31**, 3743 (1998).
- [24] W. Gordon, *Z. Phys.* **40**, 117 (1926).
- [25] D. M. Wolkow, *Z. Phys.* **94**, 250 (1935).
- [26] H. R. Reiss, *Phys. Rev. A* **22**, 1786 (1980).
- [27] A. B. Voitkiv and J. Ullrich, *J. Phys. B* **34**, 4383 (2001).
- [28] H. J. Korsch, A. Klumpp, and D. Witthaut, *J. Phys. A: Math. Gen.* **39**, 14947 (2006).
- [29] B. H. Bransden and C. J. Joachain, *Introduction to Quantum Mechanics* (Longman Scientific and Technical, Harlow, 1989), p. 352.
- [30] A. R. Swann, D. B. Cassidy, A. Deller, and G. F. Gribakin, *Phys. Rev. A* **93**, 052712 (2016).
- [31] P. Martin, V. Veniard, A. Maquet, P. Francken, and C. J. Joachain, *Phys. Rev. A* **39**, 6178 (1989).
- [32] D. Cassidy, *Eur. Phys. J. D* **72**, 53 (2018).
- [33] J. Mitroy, *Phys. Rev. A* **52**, 2859 (1995).
- [34] J. Mitroy and G. Ryzhikh, *J. Phys. B* **30**, L371 (1997).
- [35] M. Dufour, M. Valdes, R. Lazauskas, and P.-A. Hervieux, *Hyperfine Interact.* **239**, 41 (2018).
- [36] A. Y. Abul-Magd and M. H. Simbel, *Z. Phys. A* **215**, 121 (1968).
- [37] S. Mariazzi, R. Caravita, C. Zimmer, B. Rienäcker, A. Camper, A. Belov, G. Bonomi, R. S. Brusa, F. Castelli, G. Consolati, M. Doser, H. Gjersdal, L. T. Glöggler, F. Guatieri, S. Haider, V. Matveev, G. Nebbia, P. Nedelec, D. Pagano, L. Penasa *et al.*, *J. Phys. B* **54**, 085004 (2021).
- [38] A. Deller, D. Edwards, T. Mortensen, C. A. Isaac, D. P. van der Werf, H. H. Telle, and M. Charlton, *J. Phys. B* **48**, 175001 (2015).
- [39] O. Morandi, P.-A. Hervieux, and G. Manfredi, *Eur. Phys. J. D* **68**, 84 (2014).
- [40] O. Morandi, P.-A. Hervieux, and G. Manfredi, *J. Phys. B* **47**, 155202 (2014).
- [41] A. Siegman, *Lasers* (University Science Books, Sausalito, 1986).
- [42] C. Joachain, A. Makhoute, A. Maquet, and R. Taieb, *Z. Phys. D* **23**, 397 (1992).
- [43] P. Comini, P.-A. Hervieux, and F. Biraben, *Hyperfine Interact.* **228**, 159 (2014).
- [44] A. Franz and P. L. Altick, *J. Phys. B* **25**, 1577 (1992).
- [45] L. Hostler, *J. Math. Phys.* **5**, 591 (1964).
- [46] M. Abramowitz and I. A. Stegun, *Handbook of Mathematical Functions with Formulas, Graphs, and Mathematical Tables* (Dover, New York, 1964).
- [47] I. Thompson and A. Barnett, *Comput. Phys. Commun.* **36**, 363 (1985).
- [48] A. Messiah, *Quantum Mechanics* (North-Holland, Amsterdam, 1962), Vol. 2.